frontiers in Physiology

ORIGINAL RESEARCH
published: 27 October 2015
doi: 10.3389/fphys.2015.00299

Pathophysiological significance of the two-pore domain K^+ channel $K_{2P}5.1$ in splenic $CD4^+CD25^-$ T cell subset from a chemically-induced murine inflammatory bowel disease model

*Sawa Nakakura[1], Miki Matsui[1], Aya Sato[1], Mizuki Ishii[1], Kyoko Endo[1], Sayaka Muragishi[1], Miki Murase[1], Hiroaki Kito[1], Hiroki Niguma[1], Natsumi Kurokawa[1], Masanori Fujii[1], Masatake Araki[2], Kimi Araki[2] and Susumu Ohya[1]**

[1] Department of Pharmacology, Division of Pathological Sciences, Kyoto Pharmaceutical University, Kyoto, Japan, [2] Institute of Resource Development and Analysis, Kumamoto University, Kumamoto, Japan

OPEN ACCESS

Edited by:
Mauricio Antonio Retamal, Universidad del Desarrollo, Chile

Reviewed by:
Péter Béla Hajdu, University of Debrecen, Hungary
Phanindra Velisetty, University of Tennessee Health Science Center, USA

***Correspondence:**
Susumu Ohya
sohya@mb.kyoto-phu.ac.jp

Specialty section:
This article was submitted to Membrane Physiology and Membrane Biophysics, a section of the journal Frontiers in Physiology

Received: *26 May 2015*
Accepted: *09 October 2015*
Published: *27 October 2015*

Citation:
Nakakura S, Matsui M, Sato A, Ishii M, Endo K, Muragishi S, Murase M, Kito H, Niguma H, Kurokawa N, Fujii M, Araki M, Araki K and Ohya S (2015) Pathophysiological significance of the two-pore domain K^+ channel $K_{2P}5.1$ in splenic $CD4^+CD25^-$ T cell subset from a chemically-induced murine inflammatory bowel disease model. Front. Physiol. 6:299. doi: 10.3389/fphys.2015.00299

The alkaline pH-activated, two-pore domain K^+ channel $K_{2P}5.1$ (also known as TASK2/KCNK5) plays an important role in maintaining the resting membrane potential, and contributes to the control of Ca^{2+} signaling in several types of cells. Recent studies highlighted the potential role of the $K_{2P}5.1$ K^+ channel in the pathogenesis of autoimmune diseases such as rheumatoid arthritis and multiple sclerosis. The aim of the present study was to elucidate the pathological significance of the $K_{2P}5.1$ K^+ channel in inflammatory bowel disease (IBD). The degrees of colitis, colonic epithelial damage, and colonic inflammation were quantified in the dextran sulfate sodium-induced mouse IBD model by macroscopic and histological scoring systems. The expression and functional activity of $K_{2P}5.1$ in splenic $CD4^+$ T cells were measured using real-time PCR, Western blot, and fluorescence imaging assays. A significant increase was observed in the expression of $K_{2P}5.1$ in the splenic $CD4^+$ T cells of the IBD model. Concomitant with this increase, the hyperpolarization response induced by extracellular alkaline pH was significantly larger in the IBD model with the corresponding intracellular Ca^{2+} rises. The expression of $K_{2P}5.1$ was higher in $CD4^+CD25^-$ T cells than in $CD4^+CD25^+$ regulatory T cells. The knockout of $K_{2P}5.1$ in mice significantly suppressed the disease responses implicated in the IBD model. Alternations in intracellular Ca^{2+} signaling following the dysregulated expression of $K_{2P}5.1$ were associated with the disease pathogenesis of IBD. The results of the present study suggest that the $K_{2P}5.1$ K^+ channel in $CD4^+CD25^-$ T cell subset is a potential therapeutic target and biomarker for IBD.

Keywords: background K^+ channel, $K_{2P}5.1$, $CD4^+$ T cell, inflammatory bowel disease, Ca^{2+} influx, cytokine production

INTRODUCTION

Due to the overlap in the pathogeneses and pharmacological treatments, Crohn's disease (CD) and ulcerative colitis (UC) are types of inflammatory bowel diseases (IBD) (Bouma and Strober, 2003; McCole, 2014). Dextran sulfate sodium (DSS) is known to chemically induce the pathogenesis of CD and UC in rodents (Okayasu et al., 1990; Dieleman et al., 1994). A genome-wide expression profiling study showed that DSS-associated genes in mice correlated with data obtained from IBD patients (Fang et al., 2011). Therefore, the DSS-induced IBD model is a commonly used model of IBD in mice, and a number of studies have used the DSS-induced IBD model to investigate the pathogenesis of CD and UC.

An elevation in intracellular Ca^{2+} by the release of Ca^{2+} from intracellular Ca^{2+} stores and Ca^{2+} influx through store-operated Ca^{2+} channels is one of the essential triggering signals for T cell activation (Cahalan and Chandy, 2009; Hogan et al., 2010). The K^+ channel is also one of the key molecules that modulates Ca^{2+} signaling in T cells because it provides an electrochemical gradient to drive Ca^{2+} influx, and two major K^+ channels (the voltage-gated, $K_V1.3$ and intermediate-conductance Ca^{2+}-activated, $K_{Ca}3.1$) function in T and B lymphocytes (Cahalan and Chandy, 2009). Recent studies including our previous study demonstrated that the upregulation of ion channels (Orai/STIM, TRPV1, TRPA1, and $K_{Ca}3.1$) in $CD4^+$ T cells was involved in the pathogenesis of IBD, while their pharmacological blockade elicited a significant decrease in IBD disease severity (Di Sabatino et al., 2009; Di et al., 2010; Bertin et al., 2014; Kun et al., 2014; Ohya et al., 2014).

The background or leak two-pore domain K^+ (K_{2P}) channel superfamily includes 16 members and plays a crucial role in diverse physiological functions through the regulation of cell excitability (Enyedi and Czirják, 2010; Es-Salah-Lamoureux et al., 2010). The $K_{2P}5.1$ K^+ channel (also known as TASK2/KCNK5) is activated by extra- and intracellular alkalization, and plays an important role in maintaining the resting membrane potential and the control of Ca^{2+} signaling in various types of cells. $K_{2P}5.1$ has been shown to control diverse physiological and pathophysiological processes including innate immunity and cancer progression (Bittner et al., 2010b; Clark et al., 2011; Cid et al., 2013), and is, therefore, expected to become a potential therapeutic target for the treatment of autoimmune, inflammatory, and allergic diseases as well as several types of cancers. Recent studies described the pathophysiological impact of the upregulation of $K_{2P}5.1$ in $CD4^+$ and $CD8^+$ T cells on the pathogenesis of autoimmune diseases such as rheumatoid arthritis and multiple sclerosis (Bittner et al., 2010a, 2011). $K_{2P}5.1$ is inhibited by non-selective K^+ channel inhibitors such as quinidine, lidocaine, and clofilium and is activated by volatile anesthetics (Wulff and Zhorov, 2008); however, the lack of selective blockers is represents an important difficulty in experimental studies on $K_{2P}5.1$.

In the present study, we examined the involvement of the $K_{2P}5.1$ K^+ channel in $CD4^+$ T lymphocytes in the pathogenesis of IBD using a mouse model of chemically-induced IBD. We further compared histopathologies between the DSS-induced IBD model using wild-type and $K_{2P}5.1$-deficient mice.

Abbreviations: K_{2P}, two-pore domain K^+ (channel); TASK, TWIK-related acid-sensitive K^+ (channel); TWIK, tandem of P-domains in a weakly inward rectifying K^+ (channel); TALK, TWIK-related alkaline pH-activated K^+ (channel); IBD, inflammatory bowel disease; DSS, dextran sodium sulfate; HEPES, 4-(2-hydroxyethyl)-1-piperazineethanesulfonic acid; $DiBAC_4(3)$, bis-(1,3-dibutylbarbituric acid)trimethine oxonol; Fura 2-AM, acetoxymethyl 2-[5-[bis[(acetoxymethoxy-oxo-methyl)methyl]amino]-4-[2-[2-[bis[(acetoxymethoxy-oxo-methyl)methyl]amino]-5-methyl-phenoxy]ethoxy]benzofuran-2-yl]oxazole-5-carboxylate; FCM, flow cytometry; IFN, interferon; IL, interleukin; pH_e, extracellular pH; CD, cluster of differentiation or Crohn's disease; UC, ulcerative colitis; FITC, fluorescein isothiocyanate; PE, Phycoerythrin; 2-APB, 2-aminoethoxydiphenyl borate; Orai, Ca^{2+} release-activated Ca^{2+} (channel); STIM, stromal interaction molecule; TRPV, transient receptor potential, vanilloid; TRPA, transient receptor potential, subfamily A; K_{Ca}, Ca^{2+}-activated K^+ (channel); K_V, voltage-gated K^+ (channel).

MATERIALS AND METHODS

Preparation of the Dextran Sulfate Sodium (DSS)-induced Mouse IBD Model

Male C57BL/6J (6–7 weeks of age) mice were purchased from Shimizu Laboratory Supplies (Kyoto, Japan), and were acclimatized for 1 week before the experiment. They were given distilled water containing 5.0% (wt/vol) dextran sulfate sodium 5000 (DSS) (Wako Pure Chemical, Osaka, Japan) *ad libitum*. Control mice were given drinking water only. Seven days after the administration of DSS, mice were sacrificed, tissue samples were taken, and colitis and inflammation were assessed macroscopically and scored as previously reported (Ohya et al., 2014). All experiments were carried out in accordance with the guiding principles for the care and use of laboratory animals in Kyoto Pharmaceutical University, and the protocols were approved by the committee on the Ethics of Animal Research of Kyoto Pharmaceutical University (Permit Number: 15-12-091). $K_{2P}5.1$ heterozygous knockout mice bred in a C57BL6 background [B6;CB-Kcnk5Gt(pU-21)81Imeg] were established by the exchangeable gene trap method (Araki et al., 2014). Homozygous ($K_{2P}5.1^{-/-}$) knockout mice were generated by crossing heterozygous ($K_{2P}5.1^{+/-}$) males with $K_{2P}5.1^{+/-}$ females (Cid et al., 2013). Genomic DNA was isolated from finger or tail biopsies following a 3-h digestion at 50°C in buffer containing 50 mM Tris-HCl (pH 8.0), 100 mM EDTA, 100 mM NaCl, 0.1% SDS, and 1 mg/mL proteinase K, followed by heat inactivation. PCR was performed using the primer pairs to distinguish the *$K_{2P}5.1$* wild type (forward: 5′-GCTGAGAACAATAGGGACAG-3′ and reverse: 5′-TCACCCAGCTTTGGGATTCC-3′) and gene trapped (forward: 5′-GCTGAGAACAATAGGGACAG-3′and reverse: 5′-TACAGGCATCGTGGTGTCAC-3′). PCR conditions were as follows: 30 cycles at 94°C for 30 s, 60°C for 30 s, and 68°C for 30 s. The amplified products were separated on 1.0% agarose gels, and visualized by ethidium bromide staining. DSS-induced IBD model mice were prepared using male and female $K_{2P}5.1^{-/-}$ (6–10 weeks of age) and $K_{2P}5.1^{+/-}$ (6 weeks of age) mice.

Histological Scoring

Inflammation and crypt damage in hematoxylin and eosin (H&E)-stained sections were assessed as reported previously (Dieleman et al., 1994; Ohya et al., 2014). Briefly, for histological assessments, 1 cm of tissue collected from the distal colon was fixed in 10% buffered formalin, embedded in a paraffin block, cut into 5-μm-thick sections, and stained with H&E. The inflammation score was determined as a multiplication of the severity grade of inflammation (grade 0, none; grade 1, slight; grade 2, moderate; grade 3, severe) as well as its extent (grade 0, none; grade 1, mucosa; grade 2, mucosa, and submucosa; grade 3, transmural). The crypt damage score was determined as a multiplication of the damage grade of the crypt (grade 0, none; grade 1, basal 1/3 damage; grade 2, basal 2/3 damage; grade 3 only the surface epithelium intact; grade 4, entire crypt, and epithelium lost) and the percent area score (grade 1, 1–25%; grade 2, 25–50%; grade 3, 51–75%; grade 4, 76–100%). Data were obtained from three sections of the colon measured at least 200 μm apart per animal from four individual mice per group.

Cell Isolation, RNA Extraction, Reverse Transcription, and Real-time PCR

Total RNA was extracted and reverse transcribed from the T cells of mouse tissues (Ohya et al., 2013, 2014). Single cell suspensions were prepared by pressing the spleen (also the thymus and mesenteric lymph nodes) with a frosted grass slide and then filtering through a nylon mesh. $CD4^+$ cells were isolated from cell suspensions by Dynabeads® FlowComp™ Mouse $CD4^+$ (Invitrogen, Grand Island, NY, USA), according to the experimental manual supplied by Invitrogen, and were then collected in phosphate buffered saline (PBS) supplemented with 0.1% bovine serum albumin. A flow cytometric analysis confirmed that more than 95% of the purified T cells were $CD4^+$. $CD4^+CD25^-$ and $CD4^+CD25^+$ cells were also isolated from cell suspensions by Dynabeads® FlowComp™ Mouse $CD4^+$ $CD25^+$ Treg Cells (Invitrogen). A flow cytometric analysis confirmed that more than 90% of purified T cells were $CD4^+CD25^-$ and $CD4^+CD25^+$. The resulting cDNA products were amplified with gene-specific primers, and primers were designated using Primer Express™ software (Ver 1.5, Applied Biosystems, Foster City, CA, USA). Quantitative, real time PCR was performed using Syber Green chemistry (SYBR® *Premix Ex Taq*™ II) (TaKaRa BIO, Osaka, Japan) on an ABI 7500 sequence detector system (Applied Biosystems) as previously reported (Ohya et al., 2014). The following PCR primers for mouse clones were used for real-time PCR: $K_{2P}5.1$ (GenBank accession number: NM_021542, 722-844), amplicon = 123 bp; $K_{2P}3.1$ (AF065162, 692-812), 121 bp; $K_{2P}9.1$ (NM_001033876, 757-877), 121 bp; $K_{2P}16.1$ (NM_029006, 191-312), 122 bp; interferon (IFN)-γ (NM_008337, 222-323), 102 bp; interleukin-4 (IL-4) (NM_021283, 126-246), 121 bp; IL-10 (NM_010548, 245-355), 111 bp; CD25 (NM_008367, 522-642), 121 bp; IL-17A (NM_010552, 165-277), 113 bp; β-actin (ACTB) (NM_031144, 419-519), 101 bp. Regression analyses of the mean values of three multiplex RT-PCRs for $\log_{10}$ diluted cDNA were used to generate standard curves (Ohya et al., 2014). Unknown quantities relative to the standard curve for a particular set of primers were calculated, yielding the transcriptional quantitation of gene products relative to the endogenous standard, ACTB. The following PCR primers were used for real-time PCR to confirm the knockout of $K_{2P}5.1$ transcripts in T cells from $K_{2P}5.1^{-/-}$ mice: $K_{2P}5.1$ (NM_021542, 472-567), 96 bp.

Western Blotting

Splenic $CD4^+$ T cells were solubilized with lysis buffer with 1% SDS. The same amount of proteins (10 μg for each) were subjected to 10% SDS-PAGE (Ohya et al., 2014). The blots were incubated with an anti-$K_{2P}5.1$ antibody (G-14 or H-170, Santa Cruz Biotechnology, Santa Cruz, CA, USA), and then incubated with anti-rabbit or anti-goat horseradish peroxidase-conjugated IgG (Millipore). An enhanced chemiluminescence detection system (GE Healthcare, Buckinghamshire, England) was used to detect the bound antibody. The resulting images were analyzed by a LAS-3000mini device (Fujifilm, Tokyo, Japan). The blots were also probed with an anti-β-actin (ACTB) antibody (Medical & Biological Laboratories, Nagoya, Japan).

Measurement of the Membrane Potential and Intracellular Ca^{2+} Concentrations by Fluorescent Indicators

The membrane potential was measured using the fluorescent voltage-sensitive dye $DiBAC_4(3)$, as previously reported (Ohya et al., 2013, 2014). Glass bottom tissue culture dishes were coated with fibronectin (Wako Pure Chemical Industries, Osaka, Japan) in Ca^{2+} and Mg^{2+}-free PBS at 50 μg/mL for 1 $\mu g/cm^2$ at 4°C overnight. Cells were seeded onto fibronectin-coated dishes and cultured for 2 h at 37°C in 5% CO_2 humidified incubator. Prior to the fluorescence measurements with $DiBAC_4(3)$, cells were incubated in normal HEPES buffer containing 100 nM $DiBAC_4(3)$ for 20 min at room temperature. The cells were continuously incubated with 100 nM $DiBAC_4(3)$ throughout the experiments. In membrane potential imaging, cells loaded with $DiBAC_4(3)$ were illuminated at a wavelength of 490 nm, and fluorescence images were recorded on the ORCA-Flash2.8 digital camera (Hamamatsu Photonics, Hamamatsu, Japan). Additionally, intracellular Ca^{2+} concentrations were measured using the fluorescent Ca^{2+} indicator dye Fura 2-AM. Cells were incubated with 10 μM Fura 2-AM in normal HEPES solution for 30 min at room temperature. Cells loaded with Fura 2-AM were alternatively illuminated at wavelengths of 340 and 380 nm, and fluorescence images were recorded. The fluorescent intensity of Fura 2 was expressed as measured 340/380 nm fluorescence ratios after background subtraction. Data collection and analyses were performed using an HCImage system (Hamamatsu Photonics). Images were measured every 5 s, and the values of fluorescent intensity (F) were determined by measuring the average for 1 min (12 images).

Flow Cytometric Analysis

Cell surface markers were analyzed with BD FACSCalibur (BD Biosciences, San Jose, CA, USA), which acquired at least 10,000 events, and gated according to forward- and side-scatter (Ohya et al., 2013). Data were analyzed using CellQuest software (BD

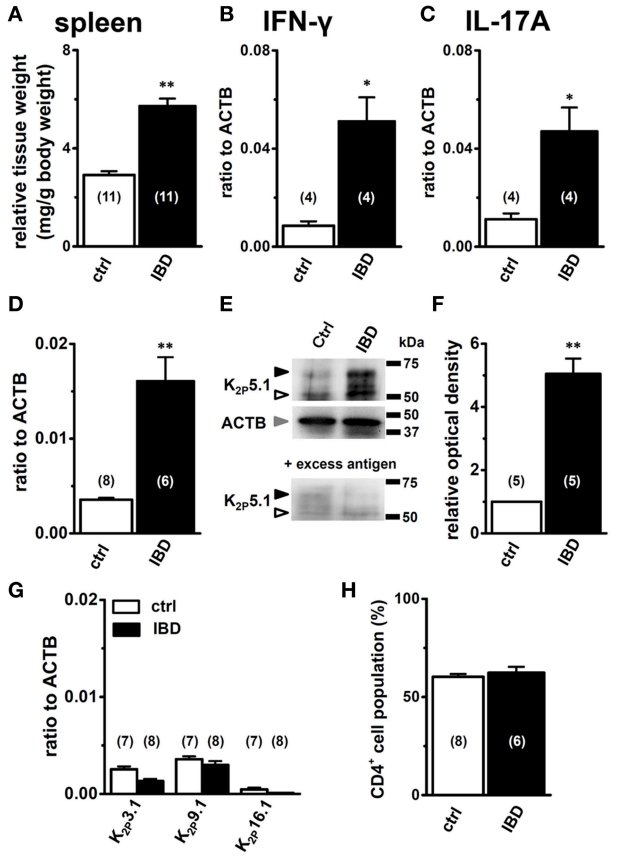

FIGURE 1 | Expression levels of $K_{2P}5.1$ and pro-inflammatory cytokines in splenic $CD4^+$ T lymphocytes of chemically-induced IBD model mice. (A) spleen weight relative to body weight in control and IBD mice. **(B–D)** quantitative, real-time PCR assay for the expression of IFN-γ **(B)**, IL-17A **(C)**, and $K_{2P}5.1$ **(D)** transcripts in the splenic $CD4^+$ cells of control and IBD model mice. Expression levels are expressed as a ratio to β-actin (ACTB). **(E)** splenic $CD4^+$ cell lysates were probed by immunoblotting with an anti-$K_{2P}5.1$ (G-14) antibody. Molecular weight standards are shown in kilodaltons (kDa) on the right. Arrowheads indicate the migrating positions of $K_{2P}5.1$ and ACTB proteins (open: $K_{2P}5.1$, closed: glycosylated $K_{2P}5.1$, gray: ACTB). Lower panel shows signals after the pre-incubation of a primary antibody with excess antigens. **(F)** summarized data obtained from **(E)** as the optical density of the band signal for $K_{2P}5.1$ (open arrowhead) in the IBD model relative to that in normal mice. **(G)** Expression of alkaline pH-activated K_{2P} K^+ channel subtype ($K_{2P}3.1$, 9.1, and 16.1) transcripts in the splenic $CD4^+$ T cells of control and IBD model mice. **(H)** the percentages of the $CD4^+$ T cell population relative to CD3+ T cells were analyzed by flow cytometry, acquiring at least 10,000 events. Results were expressed as means ± SEM. Numbers used for the experiments are shown in parentheses. *, $^{**}P < 0.05$, 0.01 vs. control mice (ctrl).

Biosciences). The lymphocyte gate was established by analyzing the forward angle vs. right angle light scatter. The percentage of positive-staining cells was determined by comparing the test histograms with those obtained using a fluorescein isothiocyanate (FITC) or phycoerythrin (PE)-conjugated anti-CD4 antibody (FITC/PE-CD4), FITC-conjugated CD3 (FITC-CD3), PE-conjugated CD8 (PE-CD8), and PE-conjugated CD25 (PE-CD25) (BD Biosciences). After being incubated with the antibodies for 1 h at room temperature, excess antibodies were removed by repeated washing with PBS.

Chemicals

The sources of pharmacological agents were as follows: clofilium tosylate (Sigma-Aldrich, Tokyo, Japan), $DiBAC_4(3)$, (Dojindo, Kumamoto, Japan), Fura 2-AM (Invitrogen), and 2-APB (Tocris Bioscience, Ellisville, MO, USA). All others were obtained from Sigma-Aldrich or Wako Pure Chemical Industries.

Statistical Analysis

Significant differences between two and among multiple groups were evaluated using the Student's *t*- and Welch's *t*-tests or Tukey's test after the *F*-test or ANOVA. Data that were non-normal distributed were analyzed using the Mann-Whitney *U*-test. Significance at $P < 0.05$ and $P < 0.01$ was indicated in the figures. Data are presented as means ± SE.

RESULTS

Upregulated Expression of the $K_{2P}5.1$ K^+ Channel in Splenic $CD4^+$ T Cells from the Mouse Model of DSS-induced Inflammatory Bowel Disease

Mice were sacrificed 7 days after the administration of 5.0% (wt/vol) DSS and tissue samples were collected. Control mice were given drinking water only. As previously reported (Ohya et al., 2014), severe macroscopic symptoms (colitis and fecal blood) were detected in DSS-induced IBD model mice, and the scores of colonic inflammation and crypt damage were significantly higher in IBD model mice than in control mice (not shown). As reported by Pereira et al. (1987), enlargement of the spleen, "splenomegaly," was detected in IBD model mice (**Figure 1A**), and a significant increase in the transcriptional expression of the Th1 cytokine interferon-γ (IFN-γ) and Th17 cytokine interleukin-17 (IL-17) was detected (**Figures 1B,C**), without any changes in the Th2 cytokine IL-4 (not shown). The flow cytometric analysis showed no significant differences of the $CD4^+$ phenotypic ratio between isolated splenic $CD3^+$ T cells from both groups (**Figure 1H**).

The quantitative, real-time PCR assay showed that the expression level of the $K_{2P}5.1$ transcripts was significantly higher in the splenic $CD4^+$ T cells of IBD model mice (IBD) than in control mice (ctrl) (**Figure 1D**). The expression levels of $K_{2P}5.1$ relative to ACTB (in arbitrary units) were 0.0036 ± 0.0002 and 0.0161 ± 0.0025 in the splenic $CD4^+$ T cells of control mice ($n = 8$) and IBD model mice ($n = 6$, $P < 0.01$), respectively. The western blot examination showed that the amount of the $K_{2P}5.1$ protein (∼50 kDa) in the cell lysate of splenic $CD4^+$ T cells was higher in IBD model mice than in control mice (**Figure 1E**, upper panel, open arrowhead), which was consistent with the results obtained by real-time PCR examination. The amount of the glycosylated $K_{2P}5.1$ protein (∼65 kDa, **Figure 1E**, upper panel, closed arrowhead) was also higher in the IBD model. The optical density for the $K_{2P}5.1$ protein band signal (∼50 kDa) relative to that for ACTB (**Figure 1E**, middle panel) was calculated using

Image J software (Ver. 1.42, NIH), and its protein expression level in control mice was expressed as 1.00. The relative optical density in the IBD model was 5.05 ± 0.48 (n = 5 for each, $P < 0.01$) (**Figure 1F**). The two band signals specific for an anti-$K_{2P}5.1$ antibody (G-14) disappeared with a pre-incubation with excess antigens (**Figure 1E**, lower panel). Similar results were obtained when another anti-$K_{2P}5.1$ antibody (H-170) was used as the primary antibody (Supplementary Figure 1). In addition, the expression levels of the other alkaline pH-activated K_{2P} channel subtypes, $K_{2P}3.1$/TASK1, $K_{2P}9.1$/TASK3, and $K_{2P}16.1$/TALK1 transcripts, were less abundant in the IBD model: <0.004 in arbitrary units (**Figure 1G**).

Enhancement in Alkaline pH_e-induced Hyperpolarizing Responses in Splenic $CD4^+$ T Cells of IBD Model Mice

To perform functional analysis of $K_{2P}5.1$ in splenic $CD4^+$ T cells, we measured the hyperpolarizing responses induced by the alkalization of extracellular pH (pH_e) (pH_e8.0 and 8.5) using the membrane potential-sensitive dye, $DiBAC_4(3)$. To confirm living cells, 140 mM high K^+-induced depolarization was measured at the end of protocol. As shown in **Figure 2A**, the fluorescence intensity of $DiBAC_4(3)$ decreased with the application of alkaline pH_e (pH_e8.5). The peak amplitude of the relative fluorescence intensity of $DiBAC_4(3)$ was lower in IBD model mice than in control mice (**Figure 2B**). When alkaline pH_e-induced hyperpolarizing responses (pH_e8.0 and 8.5) were expressed as changes in the relative fluorescence intensity of $DiBAC_4(3)$ [Δ relative fluorescence intensity of $DiBAC_4(3)$], they were significantly larger in IBD model mice than in control mice (**Figure 2C**). Under alkaline pH_e conditions, high K^+-induced increases in the fluorescence intensity of $DiBAC_4(3)$ were almost the same as those under normal pH_e (pH_e7.4) conditions (**Figure 2B**). In the presence of the non-specific $K_{2P}5.1$ blocker, clofilium (5 μM), alkaline pH_e (pH_e8.5)-induced hyperpolarizing responses disappeared in both groups. Significantly larger depolarizing responses were observed in IBD model mice (**Figure 2D**), suggesting that alkaline pH_e-induced hyperpolarizing responses via the activation of $K_{2P}5.1$ in IBD model mice were underestimated. Clofilium also inhibits voltage-gated K^+ channel $K_V1.3$, one of main K^+ channels in T cells, however, 4-aminopyridine (5 mM), a $K_V1.3$ blocker, did not induce any significant differences in the alkaline pH_e (pH_e 8.5)-induced hyperpolarizing responses [Δ relative fluorescence intensity of $DiBAC_4(3) = -0.17 \pm 0.04$ ($n = 19$)]. A recent study demonstrated that the Ca^{2+}-release activated Ca^{2+} (CRAC) channel, Orai1, which contributes to the store-operated entry of Ca^{2+} into T cells, was activated by alkaline pH (Beck et al., 2014), suggesting that the function of Orai1 was upregulated in the splenic $CD4^+$ T cells of IBD model mice. However, depolarizing responses were not suppressed by the pre-treatment with the Orai1 blocker 2-APB (10 μM) for more than 5 min ($P < 0.01$) (**Figure 2D**), and the expression levels of Orai1 transcripts were also not changed between the two groups (not shown). We subsequently observed a relationship between alkaline pH_e-induced hyperpolarization responses and $[Ca^{2+}]_i$ rises via CRAC channels in the splenic $CD4^+$ T cells of IBD model mice by simultaneously measuring $DiBAC_4(3)$ and Fura 2 signals (**Figure 2E**). As shown in **Figure 2F**, alkaline pH_e-induced hyperpolarization responses positively correlated with $[Ca^{2+}]_i$ rises in the splenic $CD4^+$ T cells of IBD model mice (R^2= 0.41). The alkaline pH_e-induced $[Ca^{2+}]_i$ rises were suppressed by about 40% by the pre-treatment with 2-APB (10 μM) (not shown).

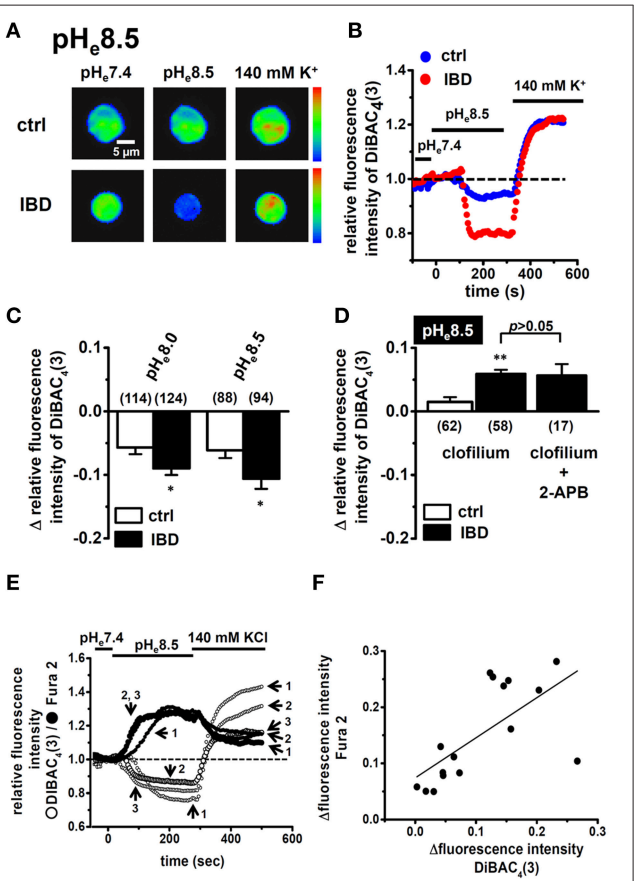

FIGURE 2 | Effects of alkaline pH_e on membrane potential and intracellular Ca^{2+} mobilization in splenic $CD4^+$ T lymphocytes of IBD model mice. (A,B) measurement of alkaline pH_e (pH_e 8.5)-induced hyperpolarizing responses in splenic $CD4^+$ T cells using the voltage-sensitive fluorescent dye $DiBAC_4(3)$. Images **(A)** are shown in pseudo-colors from blue (low intensity) to red (high intensity) in the bar. **(B)** shows the time course of changes in the fluorescence intensity of $DiBAC_4(3)$. The fluorescence intensity of $DiBAC_4(3)$ at 0 s (pH_e 7.4) is expressed as 1.0. **(C)** summarized data are shown as alkaline pH_e (pH_e 8.0 and 8.5)-induced fluorescence changes [Δrelative fluorescence intensity of $DiBAC_4(3)$] in splenic $CD4^+$ T cells of control and IBD model mice. **(D)** effects of clofilium (5 μM) and the combination of clofilium (5 μM) and 2-APB (10 μM) on alkaline-pH_e (pH_e 8.5)-induced hyperpolarizing responses in the splenic $CD4^+$ T cells of control and IBD model mice. Cells were pre-treated with clofilium and/or 2-APB for 30 min. **(E,F)** simultaneous measurements of changes in the membrane potential and intracellular Ca^{2+} concentrations by hyperpolarizing (pH_e 8.5) and depolarizing (140 mM KCl) stimulations using $DiBAC_4(3)$ and Fura 2, a Ca^{2+} indicator. **(E)** shows the time course of changes in their fluorescence intensities, and summarizing data are shown in **(F)**. Results were expressed as means ± SEM. Numbers used for the experiments are shown in parentheses. *, **P < 0.05, 0.01 vs. control mice (ctrl).

Higher Expression Level of $K_{2P}5.1$ in the Inflammatory $CD4^+CD25^-$ Subset than in the Regulatory $CD4^+CD25^+$ Subset

When $K_{2P}5.1$ is upregulated in Th1/Th17 cells producing IFN-γ/IL-17, the inhibition of $K_{2P}5.1$ may suppress the disease progression of IBD. However, when $K_{2P}5.1$ is upregulated in regulatory T cells producing IL-10, the inhibition of $K_{2P}5.1$ may promote the disease progression of IBD. In order to clarify the pathophysiological significance of the $K_{2P}5.1$ K^+ channel in IBD, we examined differences in the expression levels of $K_{2P}5.1$ between the splenic $CD4^+CD25^-$ and $CD4^+CD25^+$ subsets in IBD model mice using a real-time PCR assay. As shown in **Figure 3**, the proinflammatory Th1/Th17 cytokines IFN-γ (**Figure 3B**) and IL-17A (**Figure 3C**) transcripts were expressed at high levels in the $CD4^+CD25^-$ subset of IBD model mice, whereas the natural regulatory T cell (T_{reg}) markers CD25 (**Figure 3D**), IL-10 (**Figure 3E**), and Foxp3 (not shown) were predominantly expressed in the $CD4^+CD25^+$ subset. As shown in **Figure 3A**, $K_{2P}5.1$ transcripts were expressed at significantly higher levels in the $CD4^+CD25^-$ subset in IBD model mice than in control mice. Significant increases in the expression levels of the $K_{2P}5.1$ transcripts were also found in the $CD4^+CD25^+$ subset of IBD model mice ($P<0.01$ vs. control) (**Figure 3A**); however, these increases were significantly lower than those observed in the $CD4^+CD25^-$ subset of IBD model mice ($P < 0.01$). Correspondingly, similar levels of alkaline pH_e-induced hyperpolarizing responses (pH_e8.5) were observed in the $CD4^+CD25^-$ subset of IBD model mice but not in the $CD4^+CD25^+$ subset (not shown). These results suggested that the pharmacological inhibition of $K_{2P}5.1$ is an effective strategy for the treatment of IBD.

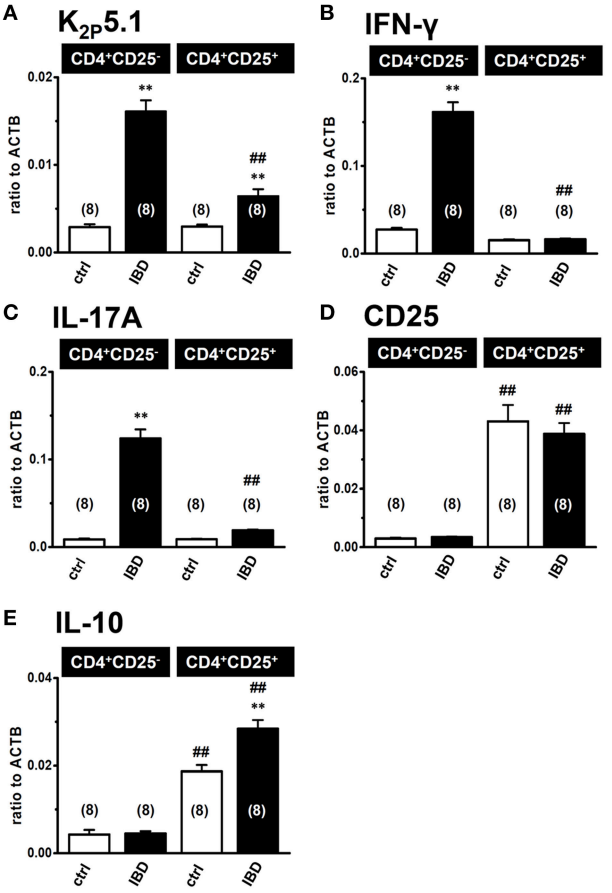

FIGURE 3 | Expression levels of $K_{2P}5.1$ and pro- and anti-inflammatory cytokine transcripts in splenic $CD4^+CD25^-$ and $CD4^+CD25^+$ subsets of IBD model mice. (A–E) real-time PCR assay for the expression of $K_{2P}5.1$ **(A)**, IFN-γ **(B)**, IL-17A **(C)**, CD25 **(D)**, and IL-10 **(E)** transcripts in the splenic $CD4^+CD25^-$ and $CD4^+CD25^+$ T cells of control and IBD model mice. Results were expressed as means ± SEM. Numbers used for the experiments are shown in parentheses. $^{**}P < 0.01$ vs. control mice (ctrl), $^{\#\#}P < 0.01$ vs. the $CD4^+CD25^-$ subset.

Decreased Susceptibility to the Pathogenesis of IBD in $K_{2P}5.1$ Knockout Mice

As described above, the lack of selective pharmacological agents represents the main difficulty in carrying out experimental studies on $K_{2P}5.1$. Therefore, we examined the effects of the genetic inhibition of $K_{2P}5.1$ on inflammatory responses during acute IBD in $K_{2P}5.1$ homozygous knockout ($K_{2P}5.1^{-/-}$) mice. As reported in our recent study (Ohya et al., 2014), severe clinical symptoms and enlargement of the spleen were observed in wild-type $K_{2P}5.1^{+/+}$ mice (**Figures 4A–C**, left columns). A significant protective effect against IBD was observed in $K_{2P}5.1^{-/-}$ mice (**Figures 4A,B**, right columns). The diarrhea scores were 2.25 ± 0.16 ($n = 8$) and 1.41 ± 0.17 ($n = 17$) in $K_{2P}5.1^{+/+}$ and $K_{2P}5.1^{-/-}$ mice, respectively ($P < 0.01$ vs. $K_{2P}5.1^{+/+}$). The degrees of splenomegaly was also significantly lower in $K_{2P}5.1^{-/-}$ mice ($P < 0.05$ vs. $K_{2P}5.1^{+/+}$). Furthermore, colonic inflammation and crypt damage were quantified by colon weight/length ratio measurements and histological scoring. As shown in **Figure 4D**, colonic wall thickening was significantly increased in $K_{2P}5.1^{+/+}$ mice, whereas no significant differences between control and IBD were observed in $K_{2P}5.1^{-/-}$ mice. Histological assessments of colonic inflammation and crypt damage also revealed that both scores were significantly lower in $K_{2P}5.1^{-/-}$ mice than in $K_{2P}5.1^{+/+}$ mice ($P < 0.01$ for the inflammation score, $P < 0.05$ for the crypt damage score) (**Figures 4E–G**). No significant differences in the degrees of colitis, colonic inflammation, or crypt damage were observed in heterozygous knockout mice ($K_{2P}5.1^{+/-}$) [diarrhea score: 1.95 ± 0.20 ($n = 22$), visible fecal blood score: 2.32 ± 0.17 ($n = 22$), inflammation score: 10.43 ± 0.87 ($n = 7$), crypt damage score: 9.86 ± 0.86 ($n = 7$)]. In $K_{2P}5.1^{-/-}$ and $K_{2P}5.1^{+/-}$ mice drinking water only for 7 days, all scores assessed in this study were 0 (not shown). In addition, in the splenic $CD4^+CD25^-$ and $CD4^+CD25^+$ cells of $K_{2P}5.1^{-/-}$ mice, the expression level of $K_{2P}5.1$ transcripts almost disappeared (**Figure 4H**), and alkaline pH_e (pH_e8.5)-induced hyperpolarizing responses were also very small in the splenic $CD4^+$ T cells of $K_{2P}5.1^{-/-}$ mice (**Figure 4I**). These results suggest that $K_{2P}5.1$ inhibitors may be efficacious in patients with IBD.

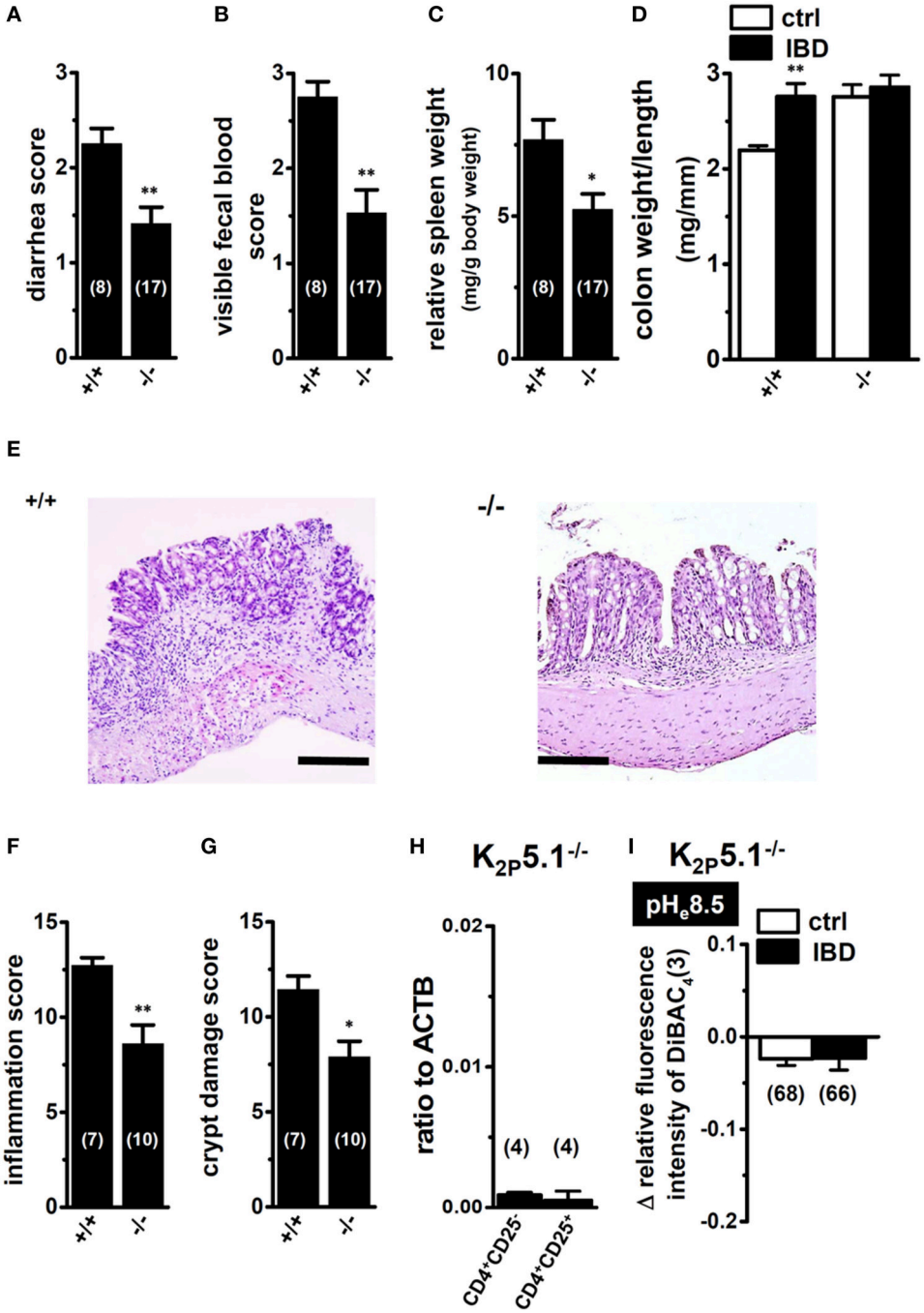

FIGURE 4 | Macroscopic disease activities and histopathological assessments in the IBD model from wild-type (+/+) and homozygous $K_{2P}5.1$ knockout (-/-) mice. (A,B) Seven days after DSS exposure, diarrhea, and visible fecal blood severities were scored on a 0–3 scale (0, Normal pellets; 1, Slightly loose feces; 2, Loose feces; 3, Watery diarrhea) and a 0–3 scale (0, Normal; 1, Slightly bloody; 2, Bloody; 3, Blood in the whole colon), respectively, in $K_{2P}5.1^{+/+}$ and $K_{2P}5.1^{-/-}$ mice. **(C)** spleen weights relative to body weights in $K_{2P}5.1^{+/+}$ and $K_{2P}5.1^{-/-}$ mice. **(D)** the colon weight/length ratio was measured in $K_{2P}5.1^{+/+}$ and $K_{2P}5.1^{-/-}$ mice. **(E–G)** Photographs of colon sections from $K_{2P}5.1^{+/+}$ and $K_{2P}5.1^{-/-}$ mice with H&E staining (magnification, X100) **(E)**. Scale bar, 100 μm. Colonic inflammation **(F)** and crypt damage **(G)** were assessed histologically. **(H)** Expression of $K_{2P}5.1$ transcripts relative to ACTB transcripts in $CD4^+CD25^-$ and $CD4^+CD25^+$ subsets from $K_{2P}5.1^{-/-}$ mice. **(I)** summarized data are shown as alkaline pH_e (pH_e 8.5)-induced hyperpolarizing responses in the splenic $CD4^+$ T cells of control and IBD model mice. Results were expressed as means ± SEM. The numbers used for the experiments are shown in parentheses. *, **$P < 0.05$, 0.01 vs. $K_{2P}5.1^{+/+}$ **(D)**.

DISCUSSION

The activation of K^+ channels in T cells promotes Ca^{2+} influx, thereby indirectly modulating Ca^{2+} signaling (Vig and Kinet, 2009). Two K^+ channel subtypes, the voltage-gated $K_V1.3$ and intermediate-conductance Ca^{2+}-activated K^+ channel $K_{Ca}3.1$, are known to mainly function in T and B lymphocytes (Di Sabatino et al., 2009). The physiological role of the two-pore domain K^+ channel $K_{2P}5.1$ was recently clarified in lymphocytes (Nam et al., 2011; Cid et al., 2013; Shin et al., 2014), and several studies have shown the pathophysiological impact of the upregulation of the two-pore domain K^+ channel $K_{2P}5.1$ in $CD4^+$ T cells on the pathogenesis of autoimmune diseases such as rheumatoid arthritis and multiple sclerosis (Bittner et al., 2010a, 2011). However, the pathophysiological impact of $K_{2P}5.1$ in diseases associated with Th1 and Th17 cytokine profiles has not yet been examined using *in vivo* animal models. This is the first study to employ chemically-induced IBD model mice to characterize the pathophysiological role of $K_{2P}5.1$ in mature $CD4^+$ T cells. The main results of the present study were as follows: (1) Facilitation of the expression level and functional activity of the $K_{2P}5.1$ K^+ channel in splenic $CD4^+$ T cells of IBD model mice, especially in the $CD4^+CD25^-$ subset (**Figures 1**, **2**), (2) Decreased disease activity index (diarrhea, bloody feces, and weight loss) and histopathological scores (colonic inflammation and crypt damage) in homozygous $K_{2P}5.1$-deficient ($K_{2P}5.1^{-/-}$) mice (**Figure 4**). We were unable to elucidate the mechanism underlying the transcription regulation of $K_{2P}5.1$ in the splenic $CD4^+$ T cells of IBD model mice. The voltage-gated K^+ channel $K_V1.3$ and Ca^{2+}-activated K^+ channel $K_{Ca}3.1$ are the main K^+ conductance channels in $CD4^+$ T cells. Although both transcripts were expressed in splenic $CD4^+CD25^-$ cells at high levels, no significant differences were observed in their expression levels between control and IBD model mice (not shown). These results suggested that the upregulation of $K_{2P}5.1$ played an important role in the changes observed in T cell Ca^{2+} signaling in IBD pathogenesis, and may affect the facilitation of proliferation and infiltration of splenic $CD4^+$ T cells. $K_{2P}5.1$ also contributes to the regulation of osmotic volume, regulatory volume decreases (RVD), in several types of cells including T cells (Niemeyer et al., 2001; Bobak et al., 2011; Andronic et al., 2013), which participate in cell cycle progression. Therefore, a dysfunction in cellular volume homeostasis via the upregulation of $K_{2P}5.1$ may also be involved in dysregulated cellular functions in the $CD4^+$ T cells of IBD model mice.

As shown in **Figure 3A**, the upregulation of $K_{2P}5.1$ was greater in splenic $CD4^+CD25^-$ T cells of IBD model mice than in $CD4^+CD25^+$ T cells. $CD4^+CD25^-$ T cells include pro-inflammatory Th1 and Th17 subsets, and an increase was observed in the transcription of IFN-γ and IL-17A in the splenic $CD4^+CD25^-$ T cells of IBD model mice (**Figures 3B,C**). Due to the lack of a selective $K_{2P}5.1$ inhibitor, we were unable to examine the effects of its *in vivo* administration on the disease activity index and histopathological scores in IBD model mice in order to clarify the pathophysiological significance of $K_{2P}5.1$ in IBD. However, we showed that the genetic knockdown of $K_{2P}5.1$ significantly protected against IBD via the amelioration of severe colitis and colonic inflammation using homozygous $K_{2P}5.1$ knockdown $K_{2P}5.1^{-/-}$ mice (**Figure 4**). Furthermore, the expression levels of the IFN-γ transcripts from the pro-inflammatory Th1 subset were significantly lower in the $CD4^+CD25^-$ cells of the IBD model from $K_{2P}5.1^{-/-}$ mice than from $K_{2P}5.1^{+/+}$ mice (**Figure 5A**), and no significant differences were noted in the expression levels of IL-17 in $CD4^+CD25^-$ cells and IL-10 in $CD4^+CD25^+$ cells between IBD models from $K_{2P}5.1^{+/+}$ and $K_{2P}5.1^{-/-}$ mice (**Figures 5B,C**). Similar findings were obtained with the genetic and pharmacological knockdown of the Ca^{2+}-activated K^+ channel $K_{Ca}3.1$ in an IBD model (Di et al., 2010; Ohya et al., 2014; Ohya and Imaizumi, 2014). It has been reported that the function of Th1 was impaired in an IBD model from $K_{Ca}3.1^{-/-}$ mice, whereas that of Th17 was normal (Di et al., 2010). We recently demonstrated the inhibition of IFN-γ transcription, but not that of IL-17A by the *in vivo* administration of selective $K_{Ca}3.1$ inhibitors in a DSS-induced IBD model (Ohya et al., 2014). Therefore, the development of small molecule $K_{2P}5.1$ modulators may represent therapeutic and/or preventative strategies for the treatment of inflammatory and autoimmune disorders and cancer, and the establishment of a novel high-throughput screening system to detect these modulators currently required (Bagriantsev et al., 2013). Furthermore, novel findings on the regulatory molecules of $K_{2P}5.1$ will provide insights into the inhibition of $K_{2P}5.1$.

Regulatory T (T_{reg}) cells play an important role in the maintenance of intestinal homeostasis, and T_{reg} cells are considered to be beneficial for IBD therapy (Boden and Snapper, 2008; Himmel et al., 2012; Gibson et al., 2013; Mayne and Williams, 2013). As shown in **Figure 3A**, the expression levels of $K_{2P}5.1$ transcripts of $K_{2P}5.1$ were significantly increased in the splenic $CD4^+CD25^+$ T cells of IBD model mice. This subset also included Foxp3-positive cells (not shown) and, thus, is referred to as naturally-occurring regulatory T cells. In B lymphocytes, the production of the anti-inflammatory cytokine IL-10 was shown to be stimulated by Ca^{2+} influx via the CRAC

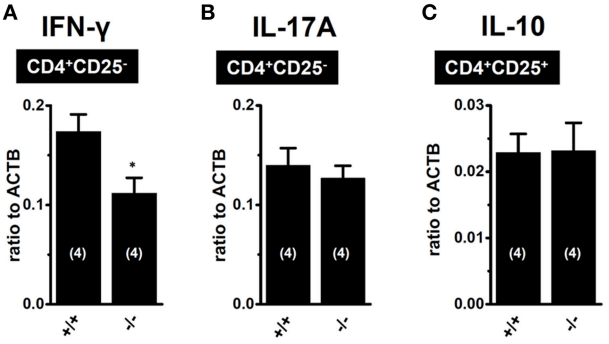

FIGURE 5 | Expression levels of IFN-γ and IL-17A transcripts in $CD4^+CD25^-$ subset of IBD models from $K_{2P}5.1^{+/+}$ (+/+) and $K_{2P}5.1^{-/-}$ (-/-) mice (A,B), and IL-10 transcripts $CD4^+CD25^+$ subset of IBD models from $K_{2P}5.1^{+/+}$ (+/+) and $K_{2P}5.1^{-/-}$ mice (-/-) (C). Expression levels were measured using a real-time PCR assay. Results were expressed as means ± SE. Numbers used for the experiments are shown in parentheses. $^*P < 0.01$ vs. $K_{2P}5.1^{+/+}$ mice.

channel (Matsumoto et al., 2011; Baba et al., 2014). Therefore, the upregulation of $K_{2P}5.1$ may strengthen the production of IL-10 in the natural T_{reg} cells of IBD model mice, and the activation of $K_{2P}5.1$ may improve the pathogenesis of IBD. In the present study, the expression of IL-10 was significantly higher in the natural T_{reg} cells of IBD model mice than in those of control mice (**Figure 3E**). No significant changes in the expression of IL-10 were found in natural T_{reg} cells of the IBD model from $K_{2P}5.1^{-/-}$ mice (**Figure 5C**); however, the long-lasting dysregulation of Ca^{2+} signaling elicited by a $K_{2P}5.1$ deficiency may be compensated by the upregulation of other K^+ channel(s), and, thus, the expression of IL-10 may be maintained within normal ranges in the T_{reg} cells of the IBD model from $K_{2P}5.1^{-/-}$ mice. Further studies are needed in order to clarify the pathophysiological role of $K_{2P}5.1$ in the natural T_{reg} cells of IBD.

In conclusion, the results of the present study suggested that the background K^+ channel $K_{2P}5.1$ in splenic $CD4^+$ T cells was involved in the pathogenesis of IBD using a chemically-induced IBD model and provided evidence for the $K_{2P}5.1$ K^+ channel as a potential therapeutic target for suppressing the progression of IBD. Dysregulated $K_{2P}5.1$ may stimulate the Th1 imbalance in the process of intestinal inflammation. The lack of selective $K_{2P}5.1$ blockers may facilitate future research on a novel high-throughput screening system to detect small molecule $K_{2P}5.1$ modulators and the regulatory mechanisms underlying $K_{2P}5.1$ transcription, translation, and protein degradation in IBD.

AUTHOR CONTRIBUTIONS

SN, HK, and SO participated in research design. SN, MM, HK, MF, and SO conducted molecular biological and biochemical experiments and performed data analyses. SN, MM, AS, MI, and HK conducted fluorescence imaging experiments and performed data analyses. SN, HN, SM, MM conducted H&E staining experiments and performed data analyses. SN, AS, HK, EK, SM, MM, NK, MA, KA, and SO contribute to the maintenance of knockout mice and preparation of IBD model mice. SN, HK, and SO contributed to the writing of the manuscript.

FUNDING

This work was supported by a Grant-in Aid for Scientific Research (C) (No. 25460111) by The Japan Society for the Promotion of Science (JSPS), a grant for the Supported Program for the Strategic Research Foundation at Private Universities, 2013-2017 (S1311035) from the Ministry of Education, Culture, Sports, Science and Technology (MEXT), the Mochida Memorial Foundation for Medical and Pharmaceutical Research, and the Uehara Memorial Foundation (to SO), a research grant from The Promotion and Mutual Aid Cooperation for Private Schools of Japan (Kyoto Pharmaceutical University and Aichi-Gakuin University).

ACKNOWLEDGMENTS

We thank to Sayo Matsuba and Toshifumi Sato for their technical assistance. $K_{2P}5.1$ heterozygous knockout mice [B6;CB-Kcnk5Gt(pU-21)81Imeg] were provided from the Center for Animal Resource and Development (CARD) (Kumamoto University, Kumamoto, Japan). Medical English Service (Kyoto, Japan) reviewed the manuscript prior to its submission.

SUPPLEMENTARY MATERIAL

The Supplementary Material for this article can be found online at: http://journal.frontiersin.org/article/10.3389/fphys.2015.00299

REFERENCES

Andronic, J., Bobak, N., Bittner, S., Ehling, P., Kleinschnitz, C., Herrmann, A. M., et al. (2013). Identification of two-pore domain potassium channels as potent modulators of osmotic volume regulation in human T lymphocytes. *Biochim. Biophys. Acta* 1828, 699–707. doi: 10.1016/j.bbamem.2012.09.028

Araki, M., Nakahara, M., Muta, M., Itou, M., Yanai, C., Yamazoe, F., et al. (2014). Database for exchangeable gene trap clones: pathway and gene ontology analysis of exchangeable gene trap clone mouse lines. *Dev. Growth Differ.* 56, 161–174. doi: 10.1111/dgd.12116

Baba, Y., Matsumoto, M., and Kurosaki, T. (2014). Calcium signaling in B cells: regulation of cytosolic Ca^{2+} increase and its sensor molecules, STIM1 and STIM2. *Mol. Immunol.* 62, 3339–3343. doi: 10.1016/j.molimm.2013.10.006

Bagriantsev, S. N., Ang, K. H., Gallardo-Godoy, A., Clark, K. A., Arkin, M. R., Renslo, A. R., et al. (2013). A high-throughput functional screen identifies small molecule regulators of temperature- and mechano-sensitive K_{2P} channels. *ACS Chem. Biol.* 8, 1841–1851. doi: 10.1021/cb400289x

Beck, A., Fleig, A., Penner, R., and Peinelt, C. (2014). Regulation of endogenous and heterologous Ca^{2+} release-activated Ca^{2+} currents by pH. *Cell Calcium* 56, 235–243. doi: 10.1016/j.ceca.2014.07.011

Bertin, S., Aoki-Nonaka, Y., de Jong, P. R., Nohara, L. L., Xu, H., Stanwood, S. R., et al. (2014). The ion channel TRPV1 regulates the activation and proinflammatory properties of $CD4^+$ T cells. *Nat. Immunol.* 15, 1055–1063. doi: 10.1038/ni.3009

Bittner, S., Bobak, N., Feuchtenberger, M., Herrmann, A. M., Göbel, K., Kinne, R. W., et al. (2011). Expression of $K_{2P}5.1$ potassium channels on $CD4^+$ T lymphocytes correlates with disease activity in rheumatoid arthritis patients. *Arthritis Res. Ther.* 13:R21. doi: 10.1186/ar3245

Bittner, S., Bobak, N., Herrmann, A. M., Göbel, K., Meuth, P., Höhn, K. G., et al. (2010a). Upregulation of $K_{2P}5.1$ potassium channels in multiple sclerosis. *Ann. Neurol.* 68, 58–69. doi: 10.1002/ana.22010

Bittner, S., Budde, T., Wiendl, H., and Meuth, S. G. (2010b). From the background to the spotlight: TASK channels in pathological conditions. *Brain Pathol.* 20, 999–1009. doi: 10.1111/j.1750-3639.2010.00407.x

Bobak, N., Bittner, S., Andronic, J., Hartmann, S., Mühlpfordt, F., Schneider-Hohendorf, T., et al. (2011). Volume regulation of murine T lymphocytes relies on voltage-dependent and two-pore domain potassium channels. *Biochim. Biophys. Acta* 1808, 2036–2044. doi: 10.1016/j.bbamem.2011.04.013

Boden, E. K., and Snapper, S. B. (2008). Regulatory T cells in inflammatory bowel disease. *Curr. Opin. Gastroenterol.* 24, 733–741. doi: 10.1097/MOG.0b013e328311f26e

Bouma, G., and Strober, W. (2003). The immunological and genetic basis of inflammatory bowel disease. *Nat. Rev. Immunol.* 3, 521–533. doi: 10.1038/nri1132

Cahalan, M. D., and Chandy, K. G. (2009). The functional network of ion channels in T lymphocytes. *Immunol. Rev.* 231, 59–87. doi: 10.1111/j.1600-065X.2009.00816.x

Cid, L. P., Roa-Rojas, H. A., Niemeyer, M. I., Gonzalez, W., Araki, M., and Sepulveda, F. V. (2013). TASK-2: a K_{2P} K^+ channel with complex regulation and diverse physiological functions. *Front. Physiol.* 4:198. doi: 10.3389/fphys.2013.00198

Clark, R. B., Kondo, C., Belke, D. D., and Giles, W. R. (2011). Two-pore domain K^+ channels regulate membrane potential of isolated human articular chondrocytes. *J. Physiol. (Lond).* 589, 5071–5089. doi: 10.1113/jphysiol.2011.210757

Di, L., Srivastava, S., Zhdanova, O., Ding, Y., Li, Z., Wulff, H., et al. (2010). Inhibition of the K^+ channel $K_{Ca}3.1$ ameliorates T cell-mediated colitis. *Proc. Natl. Acad. Sci. U.S.A.* 10, 1541–1546. doi: 10.1073/pnas.0910133107

Dieleman, L. A., Ridwan, B. U., Tennyson, G. S., Beagley, K. W., Bucy, R. P., and Elson, C. O. (1994). Dextran sulfate sodium-induced colitis occurs in severe combined immunodeficient mice. *Gastroenterology* 107, 1643–1652.

Di Sabatino, A., Rovedatti, L., Kaur, R., Spencer, J. P., Brown, J. T., Morisset, V. D., et al. (2009). Targeting gut T cell Ca^{2+} release-activated Ca^{2+} channels inhibits T cell cytokine production and T-box transcription factor T-bet in inflammatory bowel disease. *J. Immunol.* 183, 3454–3462. doi: 10.4049/jimmunol.0802887

Enyedi, P., and Czirják, G. (2010). Molecular background of leak K^+ currents: two-pore domain potassium channels. *Physiol. Rev.* 90, 559–605. doi: 10.1152/physrev.00029.2009

Es-Salah-Lamoureux, Z., Steele, D. F., and Fedida, D. (2010). Research into the therapeutic roles of two-pore-domain potassium channels. *Trends Pharmacol. Sci.* 31, 587–595. doi: 10.1016/j.tips.2010.09.001

Fang, K., Bruce, M., Pattillo, C. B., Zhang, S., Stone, R. II, Clifford, J., et al. (2011). Temporal genome wide expression profiling of DSS colitis reveals novel inflammatory and angiogenesis genes similar to ulcerative colitis. *Physiol. Genomics* 43, 43–56. doi: 10.1152/physiolgenomics.00138.2010

Gibson, D. J., Ryan, E. J., and Doherty, G. A. (2013). Keeping the bowel regular: the emerging role of Treg as a therapeutic target in inflammatory bowel disease. *Inflamm. Bowel Dis.* 19, 2716–2724. doi: 10.1097/MIB.0b013e31829ed7df

Himmel, M. E., Yao, Y., Orban, P. C., Steiner, T. S., and Levings, M. K. (2012). Regulatory T-cell therapy for inflammatory bowel disease: more questions than answers. *Immunology* 136, 115–122. doi: 10.1111/j.1365-2567.2012.03572.x

Hogan, P. G., Lewis, R. S., and Rao, A. (2010). Molecular basis of calcium signaling in lymphocytes: STIM and ORAI. *Annu. Rev. Immunol.* 38, 491–533. doi: 10.1146/annurev.immunol.021908.132550

Kun, J., Szitter, I., Kemény, A., Perkecz, A., Kereskai, L., Pohóczky, K., et al. (2014). Upregulation of the transient receptor potential anlyrin 1 ion channel in the inflamed human and mouse colon and its protective roles. *PLoS ONE* 9:e108164. doi: 10.1371/journal.pone.0108164

Matsumoto, M., Fujii, Y., Baba, A., Hikida, M., Kurosaki, T., and Baba, Y. (2011). The calcium sensors STIM1 and STIM2 control B cell regulatory function through interleukin-10 production. *Immunity* 34, 703–714. doi: 10.1016/j.immuni.2011.03.016

Mayne, C. G., and Williams, C. B. (2013). Induced and natural regulatory T cells in the development of inflammatory bowel disease. *Inflamm. Bowel Dis.* 19, 1772–1788. doi: 10.1097/mib.0b013e318281f5a3

McCole, D. F. (2014). IBD candidate genes and intestinal barrier regulation. *Inflamm. Bowel Dis.* 20, 1829–1849. doi: 10.1097/MIB.0000000000000090

Nam, J. H., Shin, D. H., Zheng, H., Lee, D. S., Park, S. J., Park, K. S., et al. (2011). Expression of TASK-2 and its upregulation by B cell receptor stimulation in WEHI-231 mouse immature B cells. *Am. J. Physiol. Cell Physiol.* 300, C1013–C1022. doi: 10.1152/ajpcell.00475.2010

Niemeyer, M. I., Cid, L. P., Barros, L. F., and Sepúlveda, F. V. (2001). Modulation of the two-pore domain acid sensitive K^+ channel TASK-2 (KCNK5) by changes in cell volume. *J. Biol. Chem.* 276, 43166–43174. doi: 10.1074/jbc.M107192200

Ohya, S., Fukuyo, Y., Kito, H., Shibaoka, R., Matsui, M., Niguma, H., et al. (2014). Upregulation of $K_{Ca}3.1$ K^+ channel in mesenteric lymph node $CD4^+$ T lymphocytes from a mouse model of dextran sodium sulfate-induced inflammatory bowel disease. *Am. J. Physiol. Gastrointest. Liver Physiol.* 306, G873–G885. doi: 10.1152/ajpgi.00156.2013

Ohya, S., and Imaizumi, Y. (2014). Intermediate-conductance Ca^{2+}-activated K^+ channel $K_{Ca}3.1$ and its related molecules in T-lymphocytes. *Inflamm. Cell Signal.* 1:e327. doi: 10.14800/ics.327

Ohya, S., Nakamura, E., Horiba, S., Kito, H., Matsui, M., Yamamura, H., et al. (2013). Role of the $K_{Ca}3.1$ K^+ channel in auricular lymph node $CD4^+$ T-lymphocyte function of the delayed-type hypersensitivity model. *Br. J. Pharmacol.* 169, 1011–1023. doi: 10.1111/bph.12215

Okayasu, I., Hatakeyama, S., Yamada, M., Ohkusa, T., Inagaki, Y., and Nakaya, R. (1990). A novel method in the induction of reliable experimental acute and chronic ulcerative colitis in mice. *Gastroenterology* 98, 694–702.

Pereira, J. L., Hughes, L. E., and Young, H. L. (1987). Spleen size in patients with inflammatory bowel disease. Does it have any clinical significance? *Dis. Colon Rectum* 30, 403–409. doi: 10.1007/BF02556485

Shin, D. H., Lin, H., Zheng, H., Kim, K. S., Kim, J. Y., Chun, Y. S., et al. (2014). HIF-1α-mediated upregulation of TASK-2 K^+ channels augments Ca^{2+} signaling in mouse B cells under hypoxia. *J. Immunol.* 193, 4924–4933. doi: 10.4049/jimmunol.1301829

Vig, M., and Kinet, J. P. (2009). Calcium signaling in immune cells. *Nat. Immunol.* 10, 21–27. doi: 10.1038/ni.f.220

Wulff, H., and Zhorov, B. S. (2008). K^+ channel modulators for the treatment of neurological disorders and autoimmune diseases. *Chem. Rev.* 108, 1744–1773. doi: 10.1021/cr078234p

Conflict of Interest Statement: The authors declare that the research was conducted in the absence of any commercial or financial relationships that could be construed as a potential conflict of interest.